Preparation of Mn_3O_4-Fe_2O_3 Composite Anode via a Molten Salts Technique and Its Application in Lithium-Ion Battery

S.H. Mohammad[a], K. Haris[a], M.F. Hassan[a*], Nurul Hayati Idris[b]

[a] School of Fundamental Science, Universiti Malaysia Terengganu,
21030 Kuala Terengganu, Terengganu, Malaysia

[b] School of Ocean Engineering, Universiti Malaysia Terengganu,
21030 Kuala Terengganu, Terengganu, Malaysia

*** Corresponding Author:**
M.F. Hassan
School of Fundamental Science, Universiti Malaysia Terengganu,
21030 Kuala Terengganu, Terengganu, Malaysia
E-mail address: mfhassan@umt.edu.my

Abstract
The Mn_3O_4-Fe_2O_3 composite was synthesized by a simple molten salts method using commercials $MnCl_2$•$2H_2O$ and $FeCl_2$•$3H_2O$ as structuring agents. The prepared composite was characterized using different analytical techniques such as Thermo gravimetric Analysis (TGA), X-ray diffraction (XRD), scanning electron microscopy (SEM) and energy dispersive spectroscopy (EDS). Experimental results indicated that the Mn_3O_4–Fe_2O_3 composite successfully synthesized at below 300ºC with a highly crystalline structure. The imaging results revealed that the morphology of composite consist of a very small clusters and a very tiny particles in a range between 100 and 1000 nm, respectively. These tiny particles were confirmed due to the existence of manganese, iron and oxygen elements. Electrochemical testing, including constant current charge-discharge was carried out. The composite contained 15% of activated carbon delivered much better electrochemical performance compared to the other two samples of 20 and 10%, respectively. The discharge capacity of 15% of activated carbon sample was calculated to be 657 mAh g^{-1}, which is higher than the sample of 20% (421 mAh g^{-1}) and 10% (55 mAh g^{-1}) after 100 cycles. The excellent electrochemical performance of sample 15% might be due to sufficiency of activated carbon in composite which provide a good contact between particles, increase electronic conductivity and accelerate the reaction of ions in chemical reduction and oxidation processes.

Keywords: Molten Salts Method, Mn_3O_4, Fe_2O_3, Composite, Anode, Lithium-ion battery

1.0 Introduction

Rechargeable lithium-ion batteries have long been considered as an attractive power source due to high energy density, low maintenance, no memory effect, no scheduled cycling needed, less self-discharge rate and a little harm when disposed, making lithium-ion well suited for modern fuel gauge applications (Chen, Yang, Fang, Zhang, & Hirano, 2013; Fu et al., 2005; Megahed & Scrosati, 1994; Min-min, Deng-jun, & Kai-yu, 2011; Takehara & Kanamura, 1993; Wang et al., 2004; Yang et al., 2012; Zhang, Song, Chen, Zhou, & Zhang, 2012). To ensure the lithium-ion battery is relevant to the current and future demands, research and development on battery electrodes needs to remain continue to ascertain that the electrodes maintain their good capacity retention, high rate capability, and safe operation over many charge-discharge cycles (Fan et al., 2004; Ji & Zhang, 2009b; Poizot, Laruelle, Grugeon, Dupont, & Tarascon, 2000; Rai, Anh, Gim, et al., 2013). In battery field, Cr, Mn, Fe, Co, Ni and Cu are the transition metal oxide compounds which are received increasing attention because of their promising electrochemical properties, such as a double theoretical capacity than carbon and safety advantage for evading the development of harmful Li dendrites (Cheng, Tao, Liang, & Chen, 2008; Fan et al., 2004; Poizot et al., 2000; Rai, Anh, Park, & Kim, 2013; Wu & Chiang, 2006), making them fascinating anode materials for LIBs. Nonetheless, the intensive researches have revealed that anodes based on pure transition metal oxides suffer serious capacity loss caused by the huge volume changes and aggregation during lithium insertion/ extraction processes resulting polarization, and slow diffusion of lithium ions and electrons in the active materials (Cheng et al., 2008; Fan et al., 2004; Lee et al., 2008; Yan et al., 2003; X. J. Zhu et al., 2009; X. Zhu, Zhu, Murali, Stoller, & Ruoff, 2011). Integration two or more compounds of transition metal oxides are anticipated to outwit these problems because the resultant composites merge the advantages of both transition metal oxides fillers, which have large Li storage capacity, low discharge potential and good interface affinity between composite particles (Cheng et al., 2008; Fan et al., 2004; Hassan, Guo, Du, Wexler, & Liu, 2009; Poizot et al., 2000). Furthermore, these transition metal oxides have highly-developed internal surface area, and large pore volume, which facilitate easy access of lithium-ions to the whole interior places of anodes, reduce lithium-ion disperse distance, and amplify severely the pace of electron transport (Bruce, Scrosati, & Tarascon, 2008; Ji & Zhang, 2009a). As a result, these composites can be promising candidates as anodes in LIBs.

In this study, we report on the preparation of manganese-iron oxides (Mn_3O_4–Fe_2O_3) composite from commercial $MnCl_2$•$2H_2O$ and $FeCl_2$•$3H_2O$ as structuring agents via a relatively simple and inexpensive molten salts technique (Hassan, Guo, Chen, & Liu, 2010; Hassan, Rahman, Guo, Chen, & Liu, 2010; Liu et al., 2010), and then coated with different amount of activated carbon. The as-prepared composite evidently improved electrochemical performance in terms of their high reversible capacities, excellent cycling performance, and good rate capability.

2.0 Material and methods

2.1 Materials

Mn_3O_4-Fe_2O_3 composite was prepared from starting materials of lithium nitrate ($LiNO_3$, 99%), lithium hydroxide monohydrate ($LiOH$•H_2O, 99%), hydrogen peroxide (H_2O_2, 32%), manganese chloride ($MnCl_2$•$2H_2O$, 98%) and iron chloride ($FeCl_3$•$6H_2O$, 99%). All chemicals were purchased from Sigma Aldrich Chemical Reagent Company and used without further purification.

2.2 Sample preparation

The starting precursors were weighted as follow: 1.7229 g (100 mmol) of $LiNO_3$, 0.2118 g (20 mmol) of $LiOH$•H_2O, 0.4047 g (10 mmol) of $MnCl_2$•$2H_2O$ and 0.6756 g (10 mmol) of $FeCl_3.6H_2O$. All precursors were mixed together and hand grinded in an agate mortar until it literally homogeneous. An amount of 1.42

g (50 mmol) of H_2O_2 was dropped cautiously under a fume hood and stirred for a few minutes. The mixture was transferred in a beaker and dried at 100°C for 24h in a vacuum oven and further heated at 300°C for 3h in a muffle furnace. The beaker was cooled down naturally before the heated sample was collected and washed for several times with distilled water and acetone using a centrifuge to remove any possible residual reactants and impurities. The product was dried in vacuum oven at 100°C for 12h, giving the final as-prepared sample.

2.3. Characterization techniques

Thermogravimetric analysis (TGA) was carried out with Mettler Toledo TGA/SDTA851^e and recorded under air at a heating rate of 10°C min^{-1}. X-ray diffraction (XRD) patterns of the as-prepared products were recorded on a MiniFlex II diffractometer equipped with an X'celerator using CuKα radiation (λ) 0.1542 nm, operated at 40 kV and 40 mA in the 2θ range between 20° and 80°. Scanning electron microscopy (SEM) observations and energy dispersive spectroscopy (EDS) measurements were carried out on a JSM 6360LA SEM. For the morphology observations, powder samples were pasted on studs and run for the gold coating to avoid the discharge problem, and then observed on a the same JSM 6360LA SEM at an acceleration voltage of 20 kV.

2.4 Electrochemical measurements

The as-synthesized material was used to prepare the electrode by mixing together Mn_3O_4–Fe_2O_3 composite, polyvinylidene fluoride (PVDF) binder, and activated carbon (AC) in 3 different weight ratios of 80:10:10 (sample A), 75:10:15 (sample B) and 70:10:20 (sample C), respectively. All the compounds were grinded together in an agate mortar. N-methylpyrrolidone (NMP) was dropped into the agate mortar to form a viscously slurry. The slurry was pasted onto Cu foils and dried in vacuum at 100 °C for 12 hours to remove the NMP solvent. The electrode was then pressed using a hydraulic pressure to enhance the contact between the copper foil, active materials, and conductive carbon. Cells were assembled in an argon-filled glove box (H_2O, O_2 < 0.1 ppm, Mbraun, Unilab, USA). The electrolyte was 1M $LiPF_6$ in a mixture of ethylene carbonate (EC) and dimethyl carbonate (DEC) (1:1 by volume, provided by MERCK KgaA, Germany), and microporous polypropylene film was used as a separator. Lithium metal foil was used as a counter electrode. The cells were galvanostatically discharged and charged using a Neware battery cycler at current density of 93 mA g^{-1} in the voltage range of 0.01- 3.0 V vs Li/Li^+.

3.0 Results and Discussion

The overall preparation procedure of Mn_3O_4–Fe_2O_3 composite is shown in Figure 1. The molten salt method has advantages such as able to produce desired materials in short period due to a fast response rate among ion species (high ionic diffusion rate) and particle morphology can be controlled easily at a low temperature (Tang, Yang, Liu, Kasaishi, & Ooi, 2002). Additionally, the low melting point of salts can prevent the development of composite particles in large size structure. Finally, the unreacted salts surrounding the composite particles were washed away by de-ionized water and acetone, leaving pores behind, and thus generating a very-fine porous structure.

Figure 2 shows a thermogravimetric Curve of the as-prepared sample. In order to examine the thermal stability of Mn_3O_4–Fe_2O_3 composite, thermogravimetric analysis (TGA) was carried out between 100 and 305°C. It reveals that there is a three-stage weight loss process. As seen in Fig. 2, the region (i) represents the first weight loss with 6% of total weight of sample observed up to 175 °C, and this loss might be attributed to the consecutive loss of water molecules from the surface of tested sample. The second weight loss is at the region (ii) with the calculated weight loss of 6 % occurred in 175 to 212°C which is

corresponded to the decomposition, volatilization and oxidation of the salts. Another 2% weight loss is found in region (iii) (213–305°C), which attributes to the formation of Mn_3O_4–Fe_2O_3 composite.

The X-ray diffractogram for Mn_3O_4–Fe_2O_3 composite powder is shown in Figure 3. The appearance of characteristic peak indicates the as-prepared powder is highly crystalline structure and identified as a co-existence of Mn_3O_4 and Fe_2O_3 phases. The significant peaks of Mn_3O_4 can be observed at 2θ = 27.59, 30.88, 33.28, 36.75, 38.62, 39.51, 50.90 and 64.43° which can be assigned to the (200), (112), (211), (202), (103), (220), (312), and (224) planes, and is good agreement with a tetragonal structure (JCPDS 75-1560). The peaks of Fe_2O_3 which located at 2θ = 23.14, 24.74, 29.90, 41.11, 42.18, 43.78, 45.92, 50.01, 54.91, 58.64, 60.24, 62.91, 72.08 and 75.28° could be assigned to the (100), (005), (006), (11-1), (11-2), (113), (11-4), (203), (11-7), (11-8), (027), (11-9), (0210) and (12-7) which might be indexed to a hexagonal structure (JCPDS 76-1821).

Figure 4 illustrates typical SEM images of Mn_3O_4–Fe_2O_3 composite structure at different location. The morphology of the sample at low magnification (Fig. 4(a)) is composed of the large agglomerated clusters with the size is between 5 and 20 μm. At higher magnification, (Fig. 4(b)), the morphology of composite consists of small groups of clusters (400–1000 nm) and it is also can be observed that, in each clusters there was a combination of very small particles with roughly standardized in size, estimated less than 100 nm as seen in Fig. 4(c). The particle morphology experimental was either spherical or cubic like with irregular shapes. Additionally, the results also indicate that the as-prepared composite has a very fine structure with porous architecture among the particles as shown in the Fig. 4(c) and 4(d) (schematic diagram of composite). Clearly, this result demonstrated successfully synthesizing Mn_3O_4–Fe_2O_3 composite structure through the simple and low-temperature synthesis technique.

The EDX result of the as-prepared composite is presented in Figure 5. There are many white, green and red spots covering majority of the area can be seen in the Figure 5(b), which is corresponding to the manganese element. The black spot in the figure is referring to the carbon tape used to adhesive the tested powder. The iron element in Figure 5(c) associated to the red, white and only few spot of green were exist. In Figure 5(d), the element of oxygen is associated to white, green and red spots that mass spreading on surface of the observed image and only small area which covered by the black spot of carbon tape. From the results, it can be confirmed that the presence of Mn and O elements in the powder is in good agreement to the XRD analyses in this study. Figure 5(e) shows the energy dispersive X-ray (EDX) spectrum of Mn_3O_4–Fe_2O_3 composite powder. The spectrum illustrates that the molten salt technique produces the compound of Mn_3O_4 and Fe_2O_3. Considering this EDX spectrum coincides with the XRD result shown before, it can confirm that the product is a mixture of Mn_3O_4 and Fe_2O_3 compounds.

Figure 6 demonstrates the first and the second charge-discharge profiles of Mn_3O_4–Fe_2O_3 anode. The sample A delivers a reversible capacity of 168 mAh g^{-1} and 136 mAh g^{-1} in the first and second cycles, respectively. The reversible capacities in the first and second cycles of sample C are 576 and 539 mAh g^{-1}, while the sample B shows the highest reversible capacities of 1327 and 1206 mAh g^{-1}, respectively. Considering the capacity of the first charge-discharge curve for all samples, the calculated initial Coulombic efficiency found that the sample B has approximately 87.3% efficiency, which is much higher than that of sample A (61.9%) and sample C (71%).

The cycling performance of samples A, B and C in the voltage range of 0.01–3.0 V is depicted in Figure 7. The sample C demonstrates a higher capacity and a great enhancement of the capacity retention. It delivers a reversible capacity of 538 mAh g^{-1} at the cycle of 51st and after 100 cycles, it was measured rise to 657 mAh g^{-1}, which is significantly better than that the sample A (40 mAh g^{-1}) and sample B (136 mAh g^{-1}). As can be seen in Figure 7, the sample C is found to have a different cycling discharge curve where its line decrease with time for 51 cycles (538 mAh g^{-1}) and increase gradually onward till cycle 100th (657 mAh g^{-1}),

confirming that there is 19% capacity gained. This rise phenomenon has not been fully understood yet, but it is sort to be related to a few factors as discussed here (Hassan, Guo, Chen, & Liu, 2011). Obviously, the sample B shows better electrochemical performance compared to the sample A and sample C.

In brief, several reasons could be given for the promising electrochemical performance of the as-prepared Mn_3O_4–Fe_2O_3 composite (sample B): (1) the multiple pores, which provides further buffering against the local volume change during the Li–Mn and Li–Fe alloying/de-alloying reaction; (2) the ability of the pores to promote liquid electrolyte diffusion into the bulk of the anode and provide fast transport channels for the Li-ions; (3) the shorter diffusion length for Li insertion due to the very fine particles, with benefits in retaining the structural stability, thereby leading to good cycling performance.

4.0 Conclusions

The present study provides a novel route to fabricate Mn_3O_4–Fe_2O_3 composite using the simple solvent-assisted molten salt technique. The synthesized Mn_3O_4–Fe_2O_3 composite indicates that it has a very good crystalline morphology with small-sized particles. The electrochemical results indicate that this composite has high reversible capacity, and long cycle life because of the combinative effects of Mn_3O_4 and Fe_2O_3 matrices as well as the unique morphology and structural features of porous composite particle. Future work includes pursuing the possibilities of extending the novel active-inactive materials strategy to incorporate two or more transition metal oxide to be composite for use as anodes in LIBs.

Acknowledgment

Financial support from the Ministry of Higher Education Malaysia through the Exploratory Research Grant Scheme (ERGS–55072) is gratefully appreciated.

References

Bruce, P. G., Scrosati, B., & Tarascon, J.M. (2008). Nanomaterials for rechargeable lithium batteries. Angewandte Chemie International Edition, 47, 2930-2946.

Chen, J., Yang, L., Fang, S., Zhang, Z., & Hirano, S. (2013). Facile fabrication of graphene/Cu_6Sn_5 nanocomposite as the high performance anode material for lithium ion batteries. Electrochimica Acta, 105, 629-634.

Cheng, F., Tao, Z., Liang, J., & Chen, J. (2008). Template-Directed Materials for Rechargeable Lithium-Ion Batteries. Chemistry of Materials, 20, 667-681.

Fan, J., Wang, T., Yu, C., Tu, B., Jiang, Z., & Zhao, D. (2004). Ordered, Nanostructured Tin-Based Oxides/Carbon Composites as the Negative-Electrode Material for Lithium-Ion Batteries. Advanced Materials, 16, 1432-1436.

Fu, L.J., Liu, H., C.Li, Wu, Y.P., Rahm, E., Holze, R., & Wu, H.Q. (2005). Electrode materials for lithium secondary batteries prepared by sol–gel methods. Progress in Materials Science, 50, 881-928.

Hassan, M. F., Guo, Z., Chen, Z., & Liu, H. K. (2010). Carbon-coated MoO_3 nanobelts as anode materials for lithium-ion batteries. Journal of Power Sources, 195, 2372-2376.

Hassan, M. F., Guo, Z., Chen, Z., & Liu, H. (2011). α-Fe_2O_3 as an anode material with capacity rise and high rate capability for lithium-ion batteries. Materials Research Bulletin, 46, 858-864.

Hassan, M. F., Guo, Z., Du, G., Wexler, D., & Liu, H. (2009). Preparation of tin nanocomposite as anode material by molten salts method and its application in lithium ion batteries. Physica Status Solidi (A), 206, 2546-2550.

Hassan, M. F., Rahman, M. M., Guo, Z., Chen, Z., & Liu, H. (2010). SnO_2–NiO–C nanocomposite as a high capacity anode material for lithium-ion batteries. Journal of Materials Chemistry, 20, 9707-9712.

Ji, L., & Zhang, X. (2009). Generation of activated carbon nanofibers from electrospun polyacrylonitrile-zinc chloride composites for use as anodes in lithium-ion batteries. Electrochemistry Communications, 11, 684-687.

Lee, S.H., Kim, Y.H., Deshpande, R., Parilla, P.A., Whitney, E., Gillaspie, D.T., & Dillon, A.C. (2008). Reversible Lithium-Ion Insertion in Molybdenum Oxide Nanoparticles. Advanced Materials, 20, 3627-3632.

Liu, B., Guo, Z. P., Du, G., Nuli, Y., Hassan, M. F., & Jia, D. (2010). In situ synthesis of ultra-fine, porous, tin oxide-carbon nanocomposites via a molten salt method for lithium-ion batteries. Journal of Power Sources, 195, 5382-5386.

Megahed, S., & Scrosati, B. (1994). Lithium-ion rechargeable batteries. Journal of Power Sources, 51, 79-104.

Min-min, Z., Deng-jun, A., & Kai-yu, L. (2011). Template synthesis of MnO_2/CNT nanocomposite and its application in rechargeable lithium batteries. Transactions of Nonferrous Metals Society of China, 21, 2010-2014.

Poizot, P., Laruelle, S., Grugeon, S., Dupont, L., & Tarascon, J.M. (2000). Nano-sized transition-metal oxides as negative-electrode materials for lithium-ion batteries. Nature, 407, 496-499.

Rai, A. K., Anh, L. T., Gim, J., Mathew, V., Kang, J., Paul, B. J., & Kim, J. (2013). Facile approach to synthesize CuO/reduced graphene oxide nanocomposite as anode materials for lithium-ion battery. Journal of Power Sources, 244, 435-441.

Rai, A. K., Anh, L. T., Park, C. J., & Kim, J. (2013). Electrochemical study of NiO nanoparticles electrode for application in rechargeable lithium-ion batteries. Ceramics International, 39, 6611-6618.

Takehara, Z., & Kanamura, K. (1993). Historical development of rechargeable lithium batteries in japan. Electrochimica Acta, 38, 1169-1177.

Tang, W., Yang, X., Liu, Z., Kasaishi, S., & Ooi, K. (2002). Preparation of fine single crystals of spinel-type lithium manganese oxide by LiCl flux method for rechargeable lithium batteries. Journals of Materials Chemistry, 12, 2991-2997.

Wang, X., Gao, L., Zhou, F., Zhang, Z., Ji, M., Tang, C., & Zheng, H. (2004). Large-scale synthesis of α-$LiFeO_2$ nanorods by low-temperature molten salt synthesis (MSS) method. Journal of Crystal Growth, 265, 220-223.

Wu, M. S., & Chiang, P. C. J. (2006). Electrochemically deposited nanowires of manganese oxide as an anode material for lithium-ion batteries. Electrochemistry Communications, 8, 383-388.

Yan, H., Sokolov, S., Lytle, J. C., Stein, A., Zhang, F., & Smyrl, W. H. (2003). Colloidal-Crystal-Templated Synthesis of Ordered Macroporous Electrode Materials for Lithium Secondary Batteries. Journal of The Electrochemical Society, 150, A1102-A1107.

Yang, G., Li, Y., Ji, H., Wang, H., Gao, P., Wang, L., & Jiang, X. (2012). Influence of Mn content on the morphology and improved electrochemical properties of Mn_3O_4/MnO@carbon nanofiber as anode material for lithium batteries. Journal of Power Sources, 216, 353-362.

Zhang, H., Song, H., Chen, X., Zhou, J., & Zhang, H. (2012). Preparation and electrochemical performance of SnO_2@carbon nanotube core-shell structure composite as anode material for lithium-ion batteries. Electrochimica Acta, 59, 160-167.

Zhu, X.J., Guo, Z.P., Zhang, P., Du, G.D., Zeng, R., Chen, Z.X., & Liu, H.K. (2009). Highly Porous Reticular Tin-Cobalt Oxide Composite Thin Film Anodes for Lithium Ion Batteries. Journal of Materials Chemistry, 19, 8360–8365.

Zhu, X., Zhu, Y., Murali, S., Stoller, M. D., & Ruoff, R. S. (2011). Nanostructured Reduced Graphene Oxide/Fe_2O_3 Composite As a High-Performance Anode Material for Lithium Ion Batteries. American Chemical Society, 5, 3333–3338.

Figure and Captions

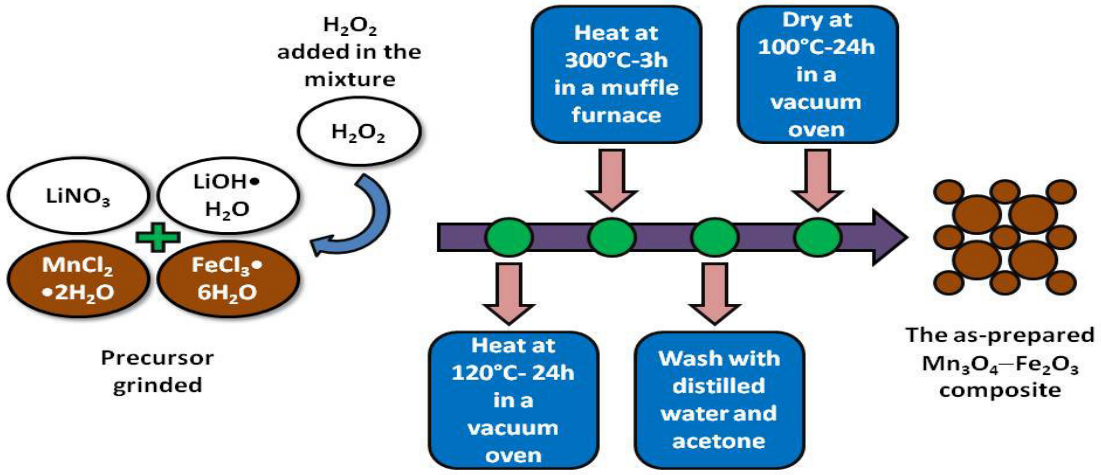

Fig. 1. Schematic diagram of a Mn_3O_4–Fe_2O_3 composite formation.

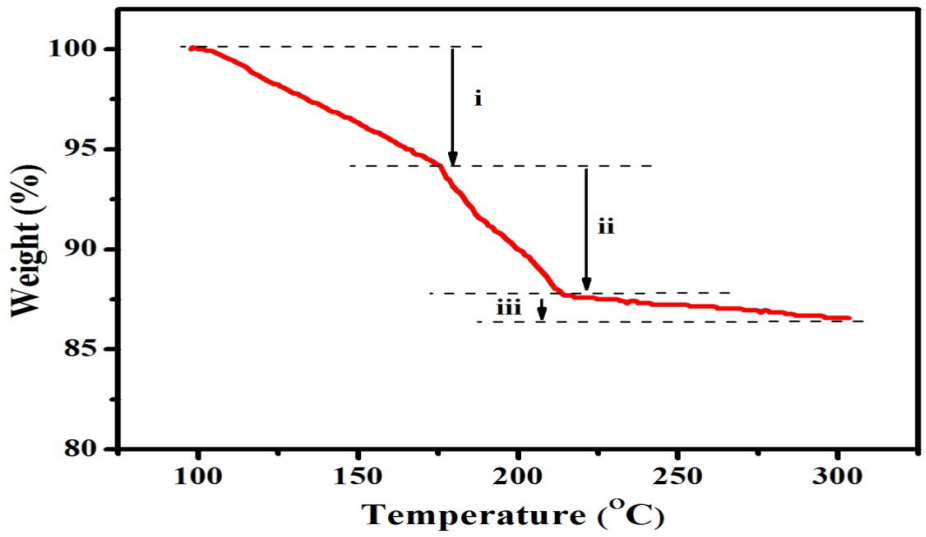

Fig. 2. TGA curve of Mn_3O_4–Fe_2O_3 composite.

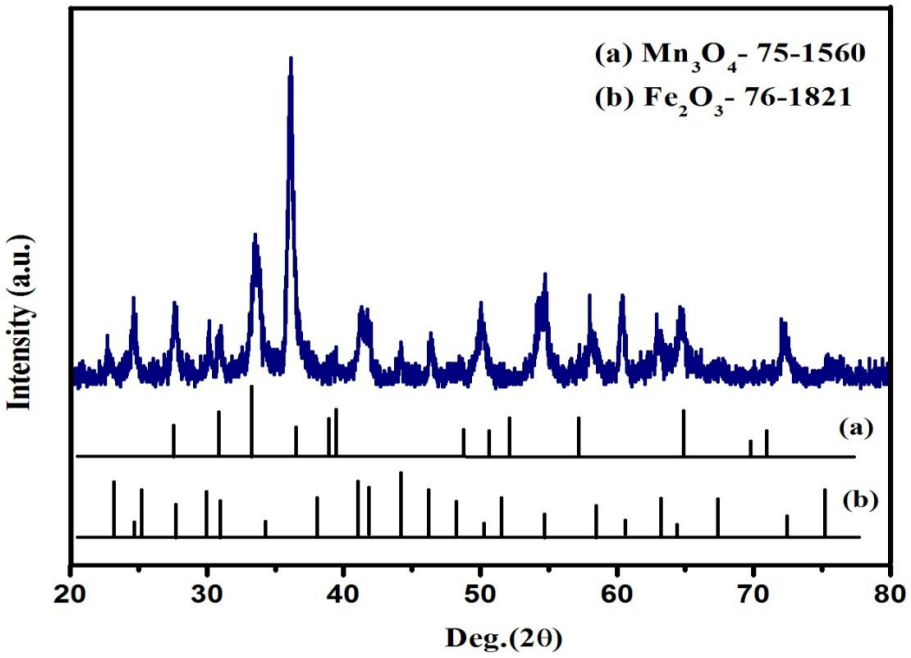

Fig. 3. X-ray diffraction pattern of the Mn_3O_4–Fe_2O_3 composite powder synthesized under molten salt conditions.

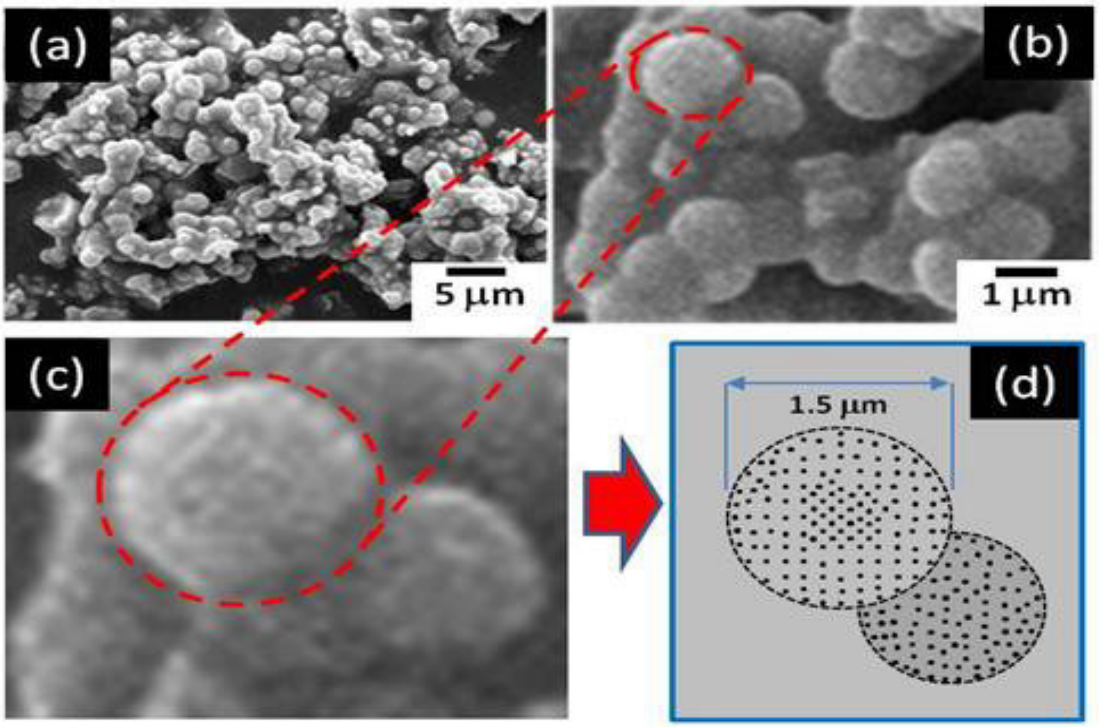

Fig. 4. Scanning electron microscope (SEM) images of Mn_3O_4–Fe_2O_3 composite. (a) low magnification image of clusters, (b) high magnification images of clusters, (c) high magnification images of individual cluster, (d) schematic diagram of individual cluster.

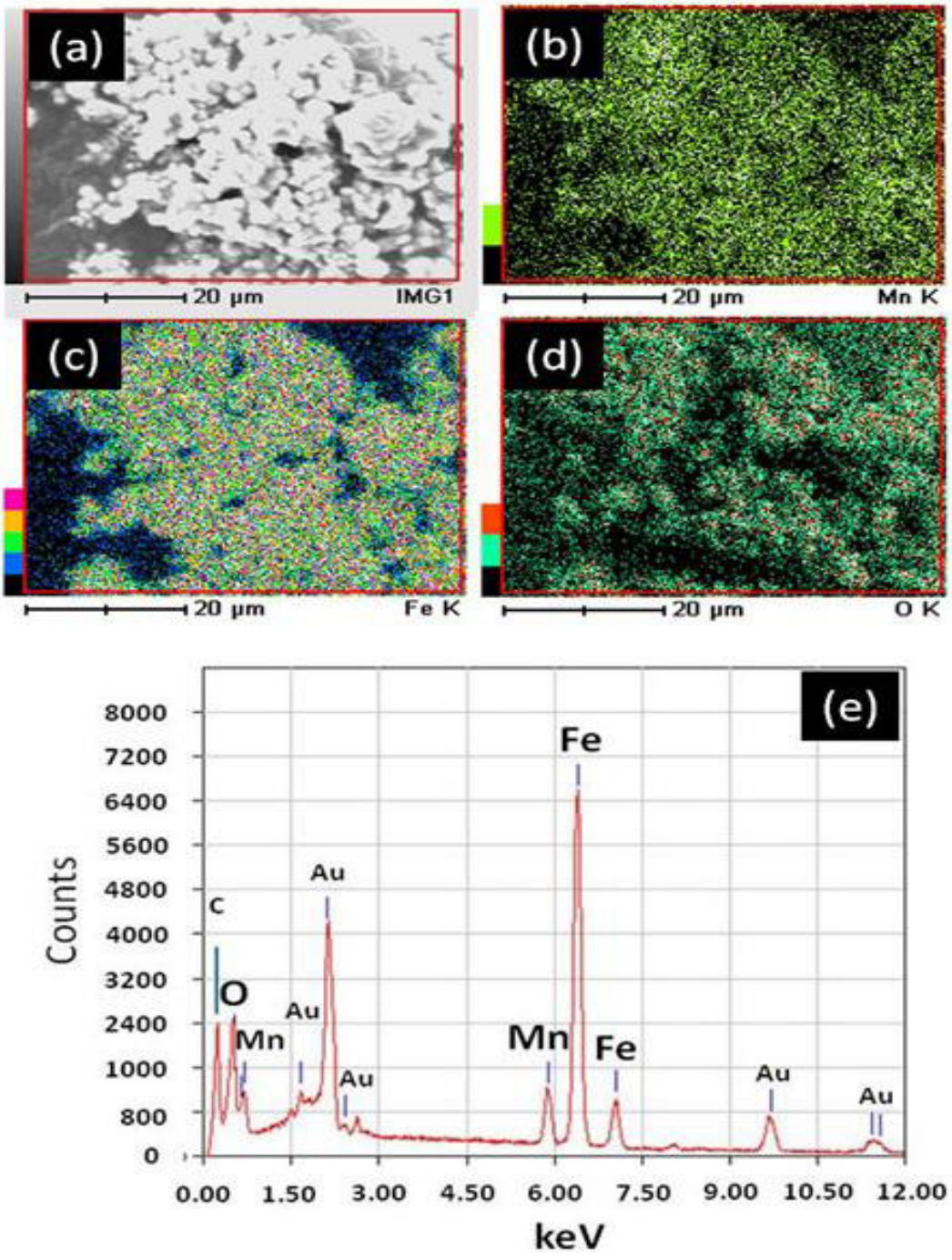

Fig. 5. EDX images of Mn_3O_4–Fe_2O_3 composite phases, (a) image, (b) Mn, (c) Fe, (d) O, and (e) EDX spectrum.

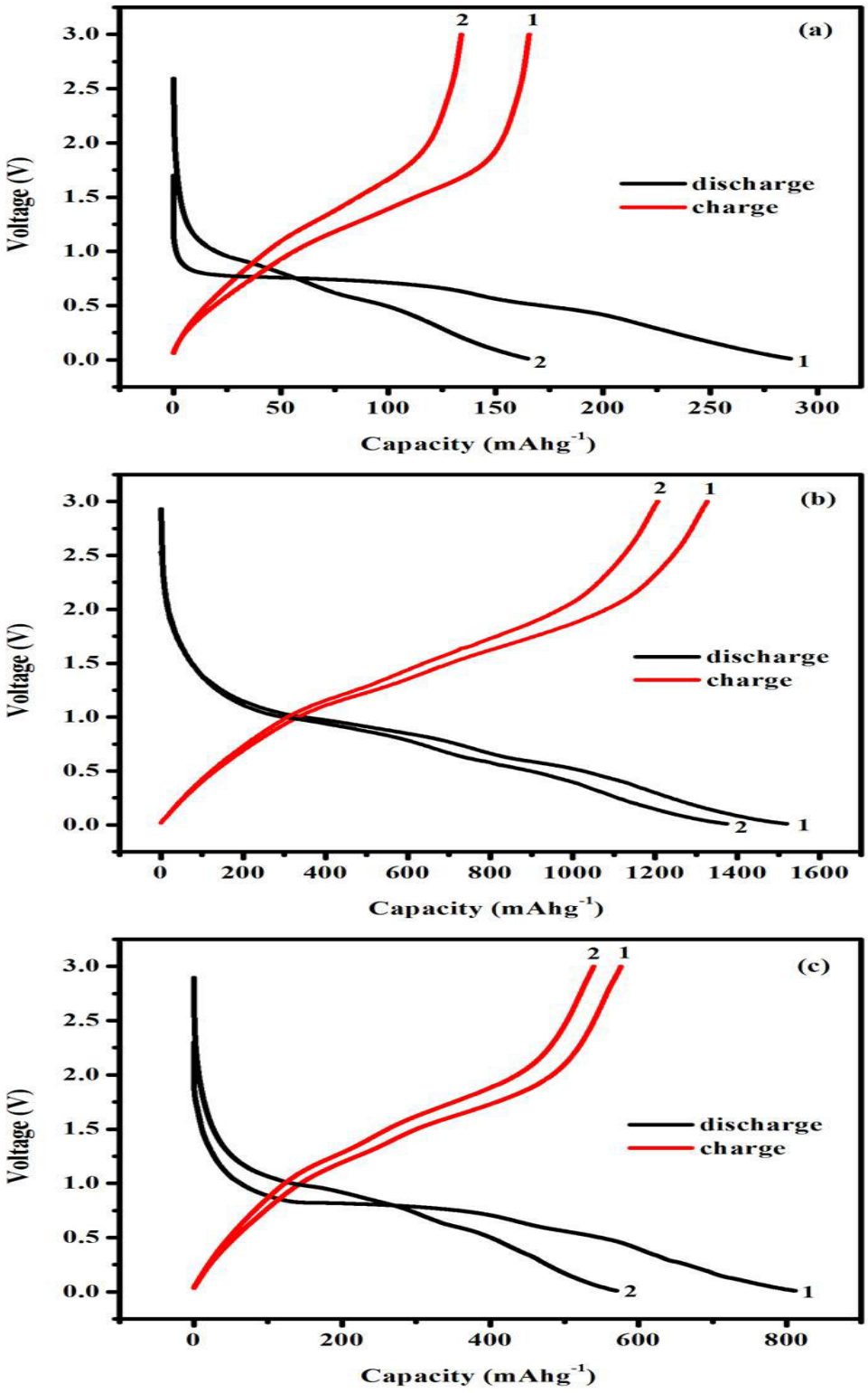

Fig. 6. The first and second charge-discharge profiles of Mn_3O_4–Fe_2O_3 composite anode of sample (a) A, (b) B, and (c) C. The cells were charged/discharged at 0.1C (94 mA g^{-1}).

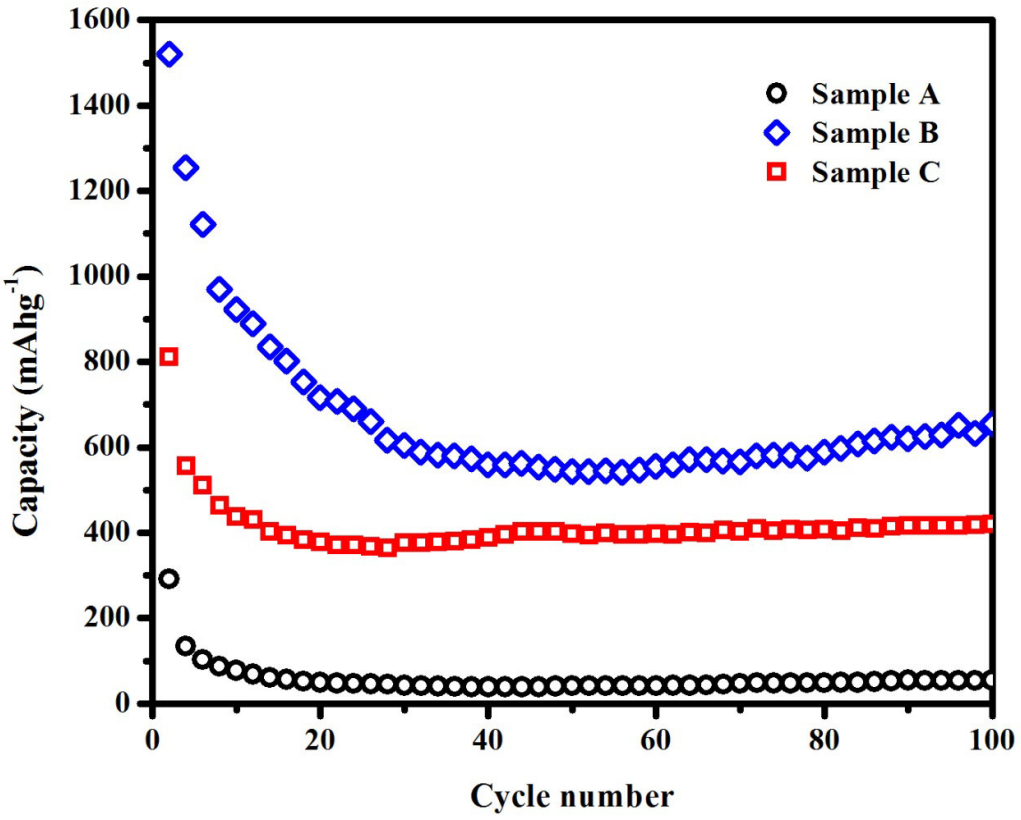

Fig. 7. Cycling performance of Mn_3O_4–Fe_2O_3 composite anodes of sample (a) A, (b) B, and (c) C. The cells were cycled at 0.1C (94 mA g^{-1}).